DEPARTMENT OF MECHANICAL ENGINEERING AND MECHANICS
COLLEGE OF ENGINEERING AND TECHNOLOGY
OLD DOMINION UNIVERSITY
NORFOLK, VIRGINIA   23529

JET VORTEX GENERATORS FOR TURBULENT FLOW SEPARATION CONTROL

By

Gregory Selby, Principal Investigator

Progress Report
For the period ended May 31, 1990

ACKNOWLEDGMENTS

JET VORTEX GENERATORS FOR
TURBULENT FLOW SEPARATION CONTROL

G. Selby

Old Dominion University, Norfolk, VA 23529-0247

J. Lin and F. Howard

NASA Langley Research Center, Hampton, VA 23665-5225

JET VORTEX GENERATORS FOR TURBULENT FLOW SEPARATION CONTROL

G. Selby*

Old Dominion University, Norfolk, VA 23529-0247

J. Lin† and F. Howard†

NASA Langley Research Center, Hampton, VA 23665-5225

Abstract

A parametric study has been performed with jet vortex generators to determine their effectiveness in controlling flow separation associated with low-speed turbulent flow over a two-dimensional rearward-facing ramp. Results indicate that flow-separation control can be accomplished, with the level of control achieved being a function of jet speed, jet orientation (with respect to the free-stream direction), and orifice pattern (double row of jets vs. single row). Compared to slot blowing, jet vortex generators can provide an equivalent level of flow control over a larger spanwise region (for constant jet flow area and speed).

Nomenclature

C_P pressure coefficient, $2(P-P_\infty)/\rho\, V_\infty^2$

C_Q total flow coefficient, $Q/\delta\lambda\, V_\infty$

D_o jet orifice diameter

Q total volumetric flow rate

R_θ Reynolds number based on momentum thickness

u' Fluctuating velocity component in the free-stream direction

V_∞ free-stream flow speed

VR ratio of jet speed to free-stream flow speed

x coordinate in the free-stream direction

α jet inclination angle (angle between the jet axis and the horizontal plane)

β jet azimuthal angle (angle between the jet axis and the free-stream direction in a horizontal plane)

δ boundary-layer thickness

θ momentum thickness

λ lateral distance between jet orifices

---

* Associate Professor
† Aerospace Engineer

1. Introduction

Trailing-edge flaps, such as the Fowler flap, double- and triple-slotted flaps, are an integral part of conventional (Boeing 707, 737 and 747) and unconventional (SST and likely, NASP) aircraft designs for lift augmentation. The increase in the effective wing area, and consequent lift increment offered by typical multielement airfoils, is highly desirable; however, there are penalties that must be accepted. [Bertin and Smith (1989)] Leading-edge flaps (e.g., Krueger) create gaps that reduce the effectiveness of laminar-flow-control (LFC) techniques. In addition, a large percentage of the volume of a wing with flaps includes support structure for the flaps. This negatively impacts the structural efficiency of the wing design.

A basic objective of the flap-system design is to attain the highest possible L/D ratio at the highest possible lift coefficient. If a clean flaps-up wing did not stall, a flap system would essentially not be needed. [Olason and Norton (1966)] For high-lift wings without flaps, the issue is clearly one of three-dimensional separation control. If effective three-dimensional low-speed separation-control techniques can be developed for implementation during aircraft take-off and landing, flaps can be omitted from aircraft designs. However, a wing without flaps (with appropriate flow-control devices) would need to be flown at a higher angle-of-attack than one with flaps, in order to create equivalent lift. Instead of placing the entire aircraft at a higher angle-of-attack, a rotating-wing design or airport "ski jumps" can be used.

Vortex generators are commonly used to alleviate boundary-layer flow separation problems in internal and external aerodynamic configurations. One commonly utilized method for flow separation control involves placing small vortex generators (rectangular, delta-shaped winglets, Wheeler-type devices, etc.) [Wheeler (1984); Rao and Kariya (1988); Selby (1989); and Lin et al. (1989, 1990)] in a spanwise array upstream of a flow separation line. In this manner, the streamwise vortices generated by the vortex

generators increase longitudinal momentum near the wall and suppress or eliminate separation.

Another method for generating longitudinal vortices is through the use of jets blown through holes in a solid surface. [Wallis (1952); Pearcey and Stuart (1959); Papell (1984); Zhang and Li (1987); and Johnston and Nishi (1989)]. These streamwise vortices can then interact with the separated flow. The holes in the surface are skewed at an angle to the free-stream direction and can be arrayed along the surface like classical vortex generators. This separated-flow control technique was first studied by Wallis (1952); however, the idea has not yet been operationally employed. Wallis (1952) demonstrated that jet vortex generators can significantly delay turbulent separation on a NACA 2214 airfoil model in low-speed flow ($V_\infty = 18.3$ m/s). Pearcey and Stuart (1959) and Zhang and Li (1987) examined the flow physics associated with jet vortex generators, including the relative strengths of the members of the vortex pair comprising a skewed jet. Papell (1984) tested jet vortex-generator orifices of circular and non-circular cross-section in a study of the fluid mechanics of the discrete hole film-cooling process as applicable to the cooling of turbine blades. Johnston and Nishi (1989) have conducted low-speed airflow experiments in a wind tunnel at a free-stream airspeed of 14.9 m/s and demonstrated that the "vortex-generator-jet" method creates longitudinal vortices that are effective in reducing the separated flow associated with a flat-plate model in an adverse pressure gradient.

Therefore, one approach to three-dimensional separation control for aircraft might involve the use of jet vortex generators. The air used in a LFC suction system near the leading-edge of a wing (operated for leading-edge-region separation control during takeoff/landing) can be bled through the jet holes (appropriately located with respect to the region of flow separation) to produce streamwise vortices that interact with and control the separated flow.

The objective of the present research is to perform a careful parametric study of jet vortex generators for low-speed two-dimensional turbulent flow-separation control. Parameters that were varied included orifice diameter, jet orientation, jet speed, longitudinal hole location, and hole pattern.

2. Experimental Apparatus and Tests

The present separation-control experiments were conducted in the NASA Langley 51x71 cm (20x28 inch) Shear-Flow Control Tunnel. This is a low-turbulence ($u'/V_\infty < .005$), subsonic, open-circuit wind tunnel. In the current study, all experiments were conducted at a free-stream speed of 40 m/s. The free-stream reference speed

was measured by a pitot-static probe mounted from the ceiling at the front of the test section.

The test-section floor was modified for the separation-control experiment. A flow-separation ramp (model) was located approximately 1.9 m from the test-section entrance. See Figure 1 for the test configuration. The tunnel floor upstream of the ramp was raised 7.6 cm to accommodate the ramp model. A suction slot at the test-section entrance was used to remove the converging-section boundary layer to eliminate any influence of upstream history on the test boundary layer. The new laminar boundary layer that developed downstream of the suction device was artificially tripped with a 5.1-cm wide strip of sandpaper (36 grit). The ceiling height of the test section was adjusted to obtain zero pressure gradient upstream of the ramp. The boundary layer just ahead of the separation ramp was fully turbulent and the thickness, δ, was approximately 3.3 cm. At this same location, the spanwise momentum thickness (θ) variation across the test plate was within ± 2.5 percent ($\theta = 3.3$ mm) and the momentum thickness Reynolds number, R_θ, was approximately 9000.

The baseline (or reference) separation model was a two-dimensional 25° ramp with a 20-cm shoulder radius as shown in Figure 2. The model spanned the entire 71-cm wide test section and produced reasonably two-dimensional flow separation at approximately the midpoint of the ramp or about 7.6 cm downstream of the horizontal tangent point (see Figure 3). Ten jet vortex generator orifices (lateral spacing of 3.0 cm) were nominally located 4.4 cm upstream of the point of horizontal tangency or 3.5δ upstream of baseline separation. The orifice diameters (D_0) tested were 0.8, 1.2, 1.6, 3.2, and 4.8 mm ($D_0/\theta = 0.24$, 0.36, 0.48, 0.97, and 1.45, respectively). Orientation of the jets was varied through changes to the jet inclination angle, α (angle between the jet axis and the horizontal plane; $15° \le \alpha \le 90°$), and the jet azimuthal angle, β (angle between the jet axis and the free-stream direction in a horizontal plane; $0° \le \beta \le 90°$). These angles are defined in Figure 4.

Twenty-five static pressure orifices were located on the centerline of the separation ramp and twenty orifices were located on the centerline of the floor downstream of the ramp. The pressure tubes for the orifices were connected to a motor-driven valve which sequentially connected each orifice to a single differential pressure gauge. All surface static pressure measurement were referenced to the free-stream static pressure measured at a location near the entrance of the test section. Spanwise pressure distributions were measured by moving the jet vortex generator assembly in the spanwise direction with respect to the (fixed) row of pressure orifices.

The "oil-dot" flow-visualization technique was used to determine surface flow patterns. A mixture of titanium

dioxide and 10 centistoke silicone oil proved to be suitable for identifying separation and reattachment lines, as shown in Figure 3. The oil dots were placed on the model surface in a square grid approximately 2.5 cm apart in both the free-stream and spanwise directions.

3. Results and Discussion

Longitudinal pressure distributions (jet orifices located symmetrically with respect to pressure orifices) are presented in Figure 5 as a function of jet orifice diameter (D_0 = 0.8, 1.2, and 1.6 mm or D_0/θ = 0.24, 0.36, and 0.48, respectively) for $\alpha = 45°$, $\beta = 90°$, and flow coefficient, $C_Q = Q/\lambda\delta V_\infty = 0.034$ with δ measured just upstream of the separation ramp. Also shown in Figure 5 are baseline (jets off) and potential flow (computed) pressure distributions. For a constant value of C_Q and variations in D_0, the velocity ratio (VR), the ratio of jet speed to free-stream speed, is variable. The best performance in terms of pressure recovery and reattachment line location was obtained with $D_0/\theta = 0.24$ (VR = 6.8). Data presented in Figure 5 generally indicate an increase in pressure recovery and a reduction in the extent of the separation region with increasing VR (decreasing D_0). When examining the baseline pressure distribution, it should be noted that the flow around a corner (or a shoulder) accelerates and decelerates symmetrically from the potential flow perspective; this is the reason for the pressure drop along the upstream portion of the shoulder. Baseline separation occurred just before the sharply increasing C_p distribution began to level off and reattachment occurred near the region of maximum C_p. The reattachment distance, therefore, can be defined as the distance between these two locations.

Figure 6 shows pressure distribution as a function of streamwise position for $D_0 = 1.6$ mm ($D_0/\theta = 0.48$, $\alpha = 45°$, and $\beta = 90°$) as a function of C_Q (or VR). These results indicate that the maximum pressure recovery was achieved at the maximum value of C_Q (or VR) when D_0 was held constant.

The effect of variations in inclination angle on the pressure recovery ($D_0/\theta = 0.24$, $C_Q = 0.034$, and $\beta = 90°$) is illustrated in Figure 7. It appears that maximum pressure recovery was obtained with $15° \leq \alpha \leq 25°$. A positive effect was also obtained with $\alpha = 45°$; however, negligible effect is shown with $\alpha = 90°$ compared with the baseline case. Surface oil-flow visualization photographs for $\alpha = 15°$ and 45°, (Figures 8 and 9, respectively) and other conditions as in Figure 7, show that the flow reattaches upstream of the baseline reattachment line for both inclination angles. However, in both cases, surface streamlines downstream of reattachment are skewed toward the (initial) direction of the jets. The skewness is greater at the lower inclination angle. For both inclination angles, the separation line is three-dimensional, with pockets of separated flow adjacent to pockets of attached flow. In addition, the separated flow appears to have a spanwise component which is stronger for $\alpha = 15°$.

Figures 10 an 11 show the effect of varying azimuthal angle on the pressure recovery with $\alpha = 15°$ and 45°, respectively ($D_0/\theta = 0.24$ and $C_Q = 0.034$). Maximum pressure recovery was achieved with $\beta = 60°$ at $\alpha = 15°$ and with $\beta = 90°$ at $\alpha = 45°$. These figures show positive effect also for $\beta = 0°$, 30°, and 90° at $\alpha = 15°$ and for $\beta = 30°$ and 60° at $\alpha = 45°$. Though there was a positive effect at $\beta = 0°$ with $\alpha = 15°$, the pressure recovery with $\alpha = 45°$ was identical to the baseline case. Pearcey and Stuart (1959) have indicated that as the jet azimuthal angle, β, is increased, one member of the pair of counter-rotating vortices comprising the jet becomes dominant and is situated close to the surface. The other weaker member of the vortex pair lies above the dominant member. Based on the present results, it appears that this "dominant" vortex was strongest at $60° \leq \beta \leq 90°$.

Measurements made to determine the spanwise variation in the pressure distribution with $D_0/\theta = 0.24$, $C_Q = 0.034$, $\alpha = 15°$, and $\beta = 90°$ are presented in Figure 12. Plane "A" passes through the centerline orifice with Planes "B", "C", and "D" being $\lambda/4$, $\lambda/2$, and $3\lambda/4$ from the centerline in the spanwise direction. These results indicate minimal spanwise variation in the streamwise pressure distributions.

The effect of the streamwise location of the jet orifices on the pressure recovery is shown in Figure 13 ($D_0/\theta = 0.24$, $C_Q = 0.034$, $\alpha = 15°$, and $\beta = 90°$). For the three cases shown, maximum pressure recovery was obtained with the jet orifices located 3δ to 10δ upstream of the reference separation line. Even with the jet orifices located 40δ upstream of the baseline separation line, significant pressure recovery was achieved, though reattachment was delayed in comparison with the reattachment location obtained with jet orifices located at 3 and 10δ.

Several configurations were examined for which adjacent jets were oriented in a manner that has been shown by Johnston and Nishi (1989) to produce counter-rotating vortices ($\beta = \pm90°$) rather than co-rotating vortices, as in the case when $\beta = $ constant for all jets. One such configuration is depicted in Figure 14 ($D_0/\theta = 0.24$, $C_Q = 0.034$, and $\alpha = 45°$), which shows that the pressure recovery was lower in the three planes examined compared with the results with $\beta = $ constant. There was also greater spanwise variability in the streamwise pressure distributions for the configuration with counter-rotating vortices than with co-rotating vortices. The results for the latter case are similar to those shown in Figure 12. Figure 15, the flow-visualization photograph for this case, shows pockets of three-dimensional separated flow on the ramp

which cause the spanwise variation in the pressure distribution. Also shown in Figure 15 are regions of surface flow in which there was early reattachment, as well as delayed separation, compared to the baseline case (Figure 3).

Several tests were conducted with the orifices arranged in two rows (5 orifices per row) as depicted in Figure 16. Jets with $D_o/\theta = 0.24$ were oriented at $\alpha = 15^\circ$ and $\beta = 90^\circ$. Results are presented in Figures 16 and 17 corresponding to values of C_Q of 0.017 and 0.034, respectively. Jets arranged in this manner are expected to be reinforcing in the streamwise direction in terms of vortex strength. Streamwise pressure distributions obtained with two rows of jets are compared to the distributions for one row of jets ($C_Q = 0.034$) in Figures 16 and 17. The double row of jets with $C_Q = 0.017$ (Figure 16) have an effective value of C_Q of 0.034. However, the pressure recovery for this double row of jets (Figure 16) was less than that for the single row shown. It is concluded that the jets arranged in a double row are non-linearly reinforced. When the jets are arranged in a double row (Figure 17) with an effective value of C_Q of 0.068, the pressure recovery for this arrangement is much less than twice the recovery for a single row. Figures 16 and 17 also show that the streamwise pressure distributions for the double row of jets exhibit spanwise uniformity. The surface oil flow visualization of the double-row configuration of Figure 17 is presented in Figure 18, which shows skewed, attached flow downstream of the ramp in the region affected by the jets. The surface flow in the near-region of the photograph is less effected by the jets due to the orientation angle of the jets.

A double row of jets arranged in the manner shown in Figures 19 and 20 (produced interacting counter-rotating vortices) was tested with $C_Q = 0.017$ and 0.034, respectively ($D_o/\theta = 0.24$ and $\alpha = 15^\circ$). As with the previous double-row configuration, the reinforcement of the jets was non-linear at both values of C_Q. With $C_Q = 0.017$ (Figure 19), the double row of jets oriented to produce counter-rotating vortices produced a level of pressure recovery comparable to that produced by the double row of jets oriented to produce co-rotating vortices (Figure 16). However, at the higher value of C_Q(0.034), the counter-rotating vortex configuration produced a maximum pressure recovery (Figure 20) less than that produced by the co-rotating vortex configuration (Figure 17), but comparable to the configuration with the single row of jets having $\beta = $ constant $= 90^\circ$. The spanwise variability in the streamwise pressure distribution shown in Figure 20 suggests that the counter-rotating vortex configuration generates a level of reinforcement that varies in the spanwise direction. The oil-flow visualization photograph (Figure 21) corresponding to the counter-rotating vortex configuration of Figure 20 shows attached flow downstream of the ramp, but pockets of three-dimensional separated flow on the ramp which resulted in the spanwise pressure variations observed.

Air injection through a 0.13 by 23.4 mm rectangular slot, oriented as shown in Figure 22 ($\beta = 0^\circ$, VR=6.8, and $C_Q = 0.034$), produced the level of pressure recovery indicated. The slot was designed with a total flow area corresponding to 10 jet orifices with $D_n/\theta = 0.24$. The pressure recovery produced by slot injection was less than that produced by jet vortex generators with $\alpha = 15$ and 45° ($\beta = 90^\circ$). In addition, Figure 23 shows that the flow is attached only in a small region near the centerline of the model, where the slot is located. To achieve flow control with slot injection comparable to that obtained with the jet vortex generators (with the same extent of spanwise treatment; i.e., longer slot) would probably require an order-of-magnitude increase in the air volumetric flow rate through the slot.

4. Conclusions

A parametric study performed with jet vortex generators has shown them to be effective in controlling flow separation associated with low-speed turbulent flow over a two-dimensional rearward-facing ramp. Specifically, the following conclusions have been drawn from the present results:

1. For given values of C_Q, α, and β, jet vortex generator performance increased with decreasing D_o due to increasing VR.

2. For given values of D_o α, and β, jet vortex generator performance increased with increasing C_Q due to increasing VR.

3. For given values of D_o, β, and C_Q, jet vortex generator performance generally increased with decreasing α, since momentum transfer occurred nearer the model wall.

4. For given values of D_o, α, and C_Q, jet vortex generator performance generally increased with increasing β up to values of 60° to 90° due to the increasing strength of the dominant member of the vortex pair comprising a skewed jet.

5. For given values of D_o, α, β, and C_Q, jet vortex generator performance generally decreased with increasing distance upstream of the separation line; however, the level of flow-separation control with jets located as far as 40δ upstream of the baseline separation line was still significant.

6. For given values of D_o, α, β, and C_Q, streamwise pressure distributions displayed spanwise uniformity for

a single row of co-rotating jets, as well as for a double row.

7. A single row (or a double row) of jets oriented to produce counter-rotating vortices (in terms of adjacent dominant vortex-pair members) were not as effective as a single row (or a double row) of jets oriented to produce co-rotating vortices, and exhibited a lower level of spanwise uniformity in the streamwise pressure distribution.

8. Jets in a double-row pattern generally reinforced non-linearly in terms of the effect on pressure recovery.

9. Slot injection produced a level of pressure recovery somewhat less than that achieved with a single row of co-rotating vortex generator jets; however, the resulting region of attached flow was very limited in spanwise extent.

10. Oil flow visualization photographs generally indicated attached flow downstream of the ramp; however, surface streamlines were usually skewed in that region, especially with the higher values of β.

11. Oil flow visualization photographs also documented the presence of pockets of three-dimensional separated flow on the ramp in the vicinity of the flow-separation region, especially for the counter-rotating vortex configurations.

12. The most effective jet vortex generator configurations tested were the single- and double-row co-rotating vortex configurations with $\alpha = 15°$ and $\beta = 90°$.

Acknowledgement

References

Bertin, J.: Smith, M. 1989: Aerodynamics for engineers. Englewood Cliffs, New Jersey: Prentice Hall.

Johnston, J.: Nishi, M. 1989: Vortex generator jets — a means for passive and active control of boundary-layer separation. AIAA Paper No. 89-0564.

Lin, J.: Howard, F.: Selby, G. 1989: Turbulent flow separation control through passive techniques. AIAA Paper No. 89-0976.

Lin, J.: Howard, F.: Selby, G. 1990: Investigation of several passive and active methods for turbulent flow separation control. AIAA Paper No. 90-1598.

Olason, M.: Norton, D. 1966: Aerodynamic design philosophy of the Boeing 737. Journal of Aircraft. 3(6), 524-528.

Papell, S. 1984: Vortex generating flow passage design for increased film-cooling effectiveness and surface coverage. NASA TM 83617.

Pearcey, H.: Stuart, C. 1959: Methods of boundary-layer control for postponing and alleviating buffeting and other effects of shock-induced separation. New York: Institute of the Aeronautical Sciences. SMF Paper No. FF-22.

Rao, D.: Kariya, T. 1988: Boundary-layer submerged vortex generators for separation control—an exploratory study. AIAA Paper No. 88-3546-CP.

Selby, G. 1989: Passive control of three-dimensional separated vortical flow associated with swept rearward-facing steps. Journal of Fluids Engineering. 11(1), 99-101.

Wallis, R. 1952: The use of air jets for boundary-layer control. Australia: Aerodynamics Research Laboratories. Aero Note 110.

Wheeler, G. 1984: Means of maintaining attached flow of a flow medium. U.S. Patent No. 4455045.

Zhang, S.: Li, F. 1987: Experiments about the air jet vortex generator. Proceedings of the 8th Institute of Aeronautics and Astronautics. Cincinnati, Ohio. 513-516.
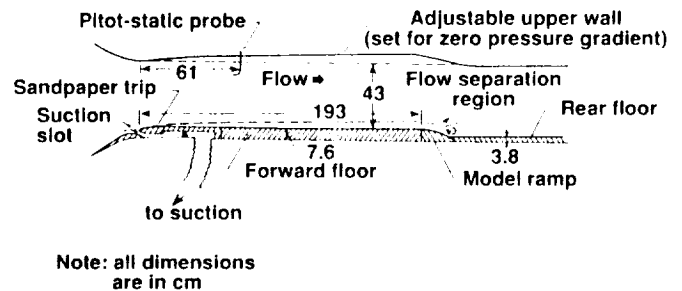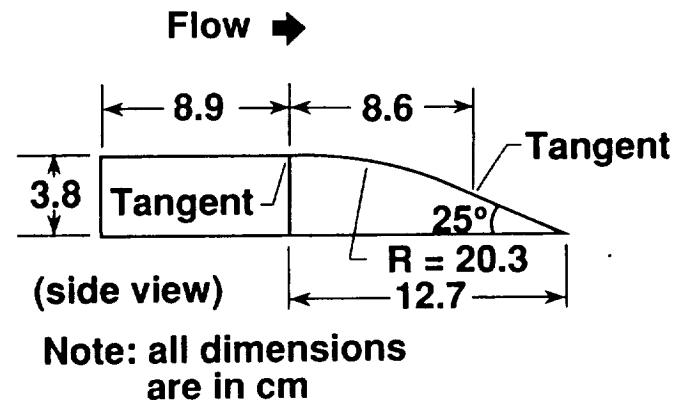

Figure 1. Test configuration in tunnel.
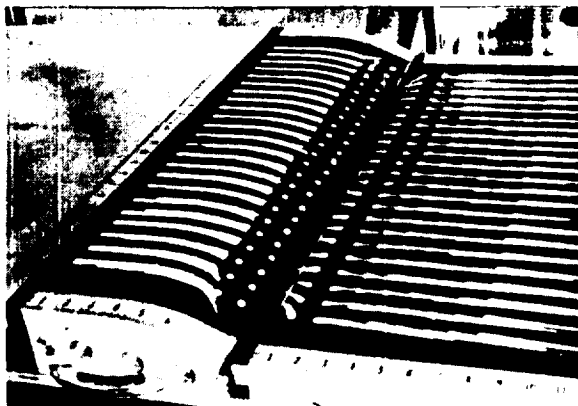

Figure 2. Geometry of the model ramp.
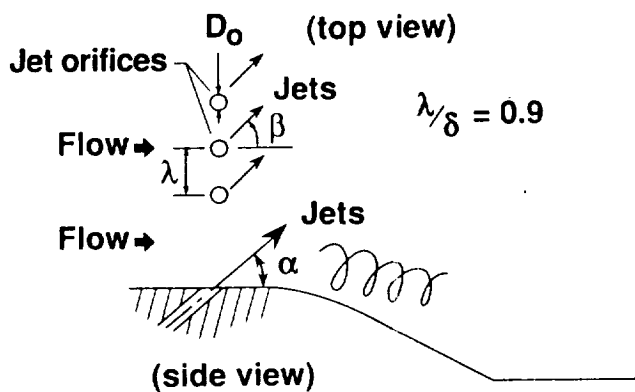
Figure 3. Oil flow visualization of baseline separation.

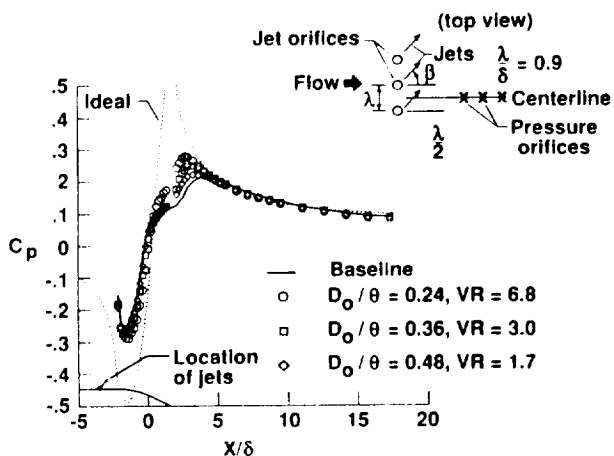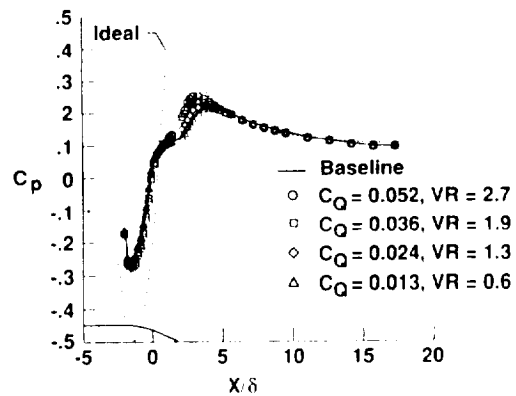Figure 6. Pressure distributions for jet vortex generators with variable C_Q for $D_o/\theta = 0.48$, $\alpha = 45^\circ$, and $\beta = 90^\circ$
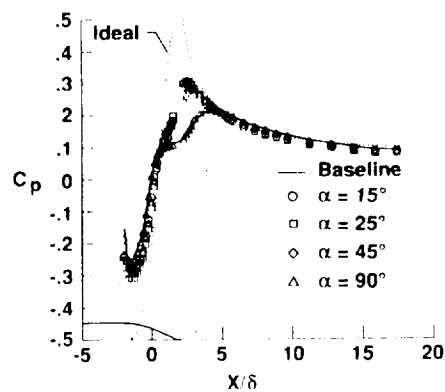
Baseline
o $C_Q = 0.052$, VR = 2.7
□ $C_Q = 0.036$, VR = 1.9
◇ $C_Q = 0.024$, VR = 1.3
△ $C_Q = 0.013$, VR = 0.6

D_o (top view)
Jet orifices
Jets
$\lambda/\delta = 0.9$
Flow
β
λ
Flow
Jets
α
(side view)

Figure 4. Geometry of jet vortex generators.

Figure 7. Pressure distributions for jet vortex generators with variable α for $D_o/\theta = 0.24$, $\beta = 90^\circ$, VR = 6.8, and $C_Q = 0.034$.

Baseline
o $\alpha = 15^\circ$
□ $\alpha = 25^\circ$
◇ $\alpha = 45^\circ$
△ $\alpha = 90^\circ$

(top view)
Jet orifices
Jets $\frac{\lambda}{\delta} = 0.9$
Flow
β
λ
Centerline
$\frac{\lambda}{2}$
Pressure orifices

Baseline
o $D_o/\theta = 0.24$, VR = 6.8
□ $D_o/\theta = 0.36$, VR = 3.0
◇ $D_o/\theta = 0.48$, VR = 1.7
Location of jets

Figure 5. Pressure distributions for jet vortex generators with variable jet D_o for $\alpha = 45^\circ$, $\beta = 90^\circ$, and $C_Q = 0.034$.

Figure 8. Oil flow visualization for jet vortex generators with $\alpha = 15^\circ$, $\beta = 90^\circ$, $D_o/\theta = 0.24$, VR = 6.8, and $C_Q = 0.034$.

Figure 9. Oil flow visualization for jet vortex generators with $\alpha = 45°$, $\beta = 90°$, $D_o/\theta = 0.24$, VR = 6.8, and $C_Q = 0.034$.

Figure 10. Pressure distributions for jet vortex generators with variable β for $\alpha = 15°$, $D_o/\theta = 0.24$, VR = 6.8, and $C_Q = 0.034$.
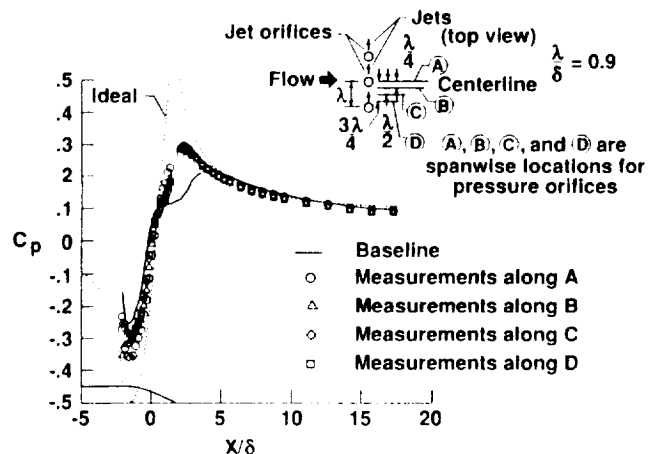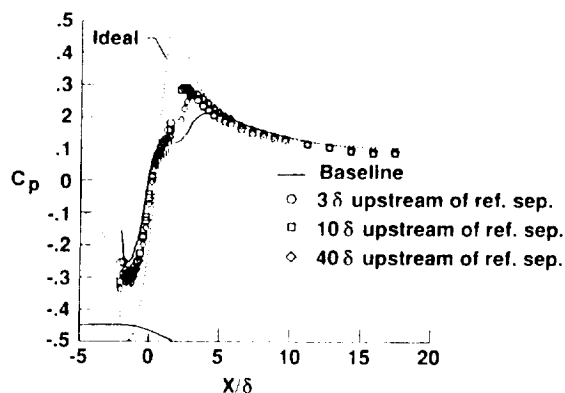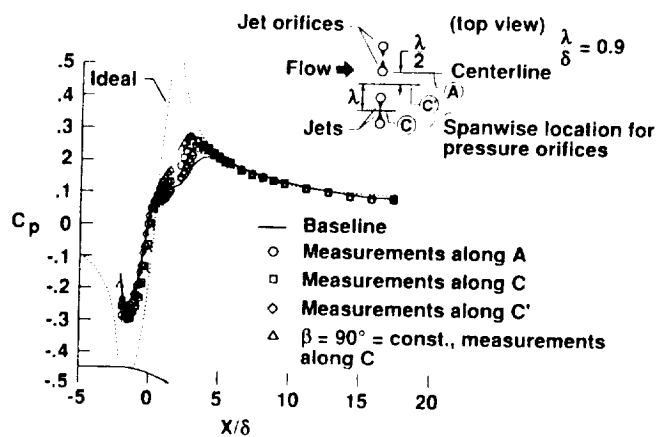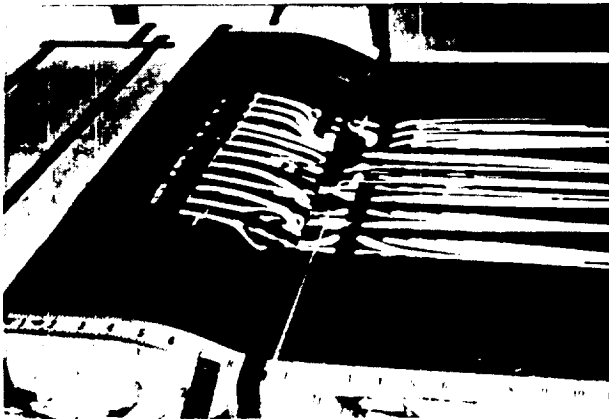

Figure 11. Pressure distributions for jet vortex generators with variable β for $\alpha = 45°$, $D_o/\theta = 0.24$, VR = 6.8, and $C_Q = 0.034$.

Figure 12. Pressure distributions for jet vortex generators at several spanwise locations with $\alpha = 15°$, $\beta = 90°$, $D_o/\theta = 0.24$, VR = 6.8, and $C_Q = 0.034$.

Figure 13. Pressure distributions for jet vortex generators at several streamwise locations with $\alpha = 15°$, $\beta = 90°$, $D_o/\theta = 0.24$, VR = 6.8, and $C_Q = 0.034$.

Figure 14. Pressure distributions at several spanwise locations for counter-rotating jet vortex generators with $\alpha = 45°$, $\beta = \pm 90°$, $D_o/\theta = 0.24$, VR = 6.8, and $C_Q = 0.034$.

Figure 15. Oil flow visualization for counter-rotating jet vortex generators with $\alpha = 45°$, $\beta = \pm 90°$, $D_o/\theta = 0.24$, VR = 6.8, and $C_Q = 0.034$.
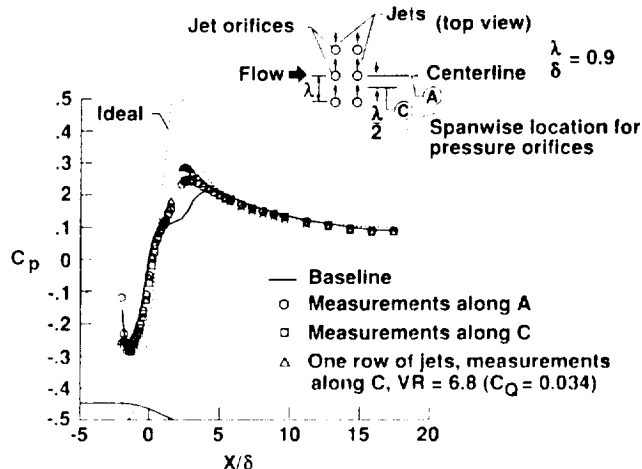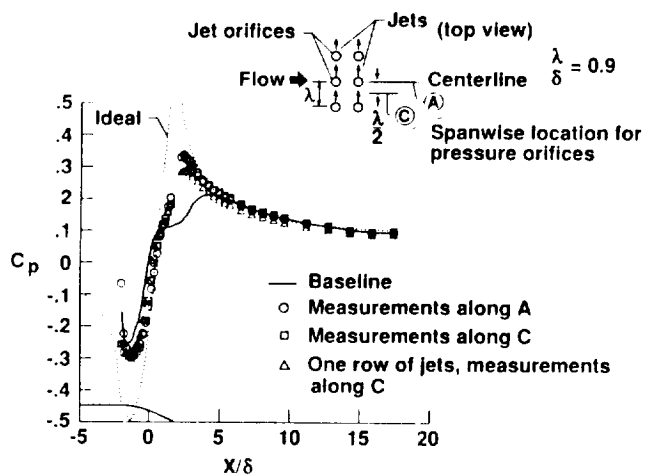

Figure 16. Pressure distributions at two spanwise locations for a double row of co-rotating jet vortex generators with $\alpha = 15°$, $\beta = 90°$, $D_o/\theta = 0.24$, VR = 3.4, and $C_Q = 0.017$.

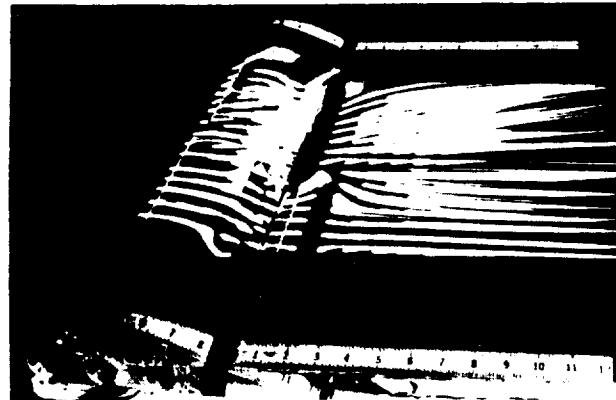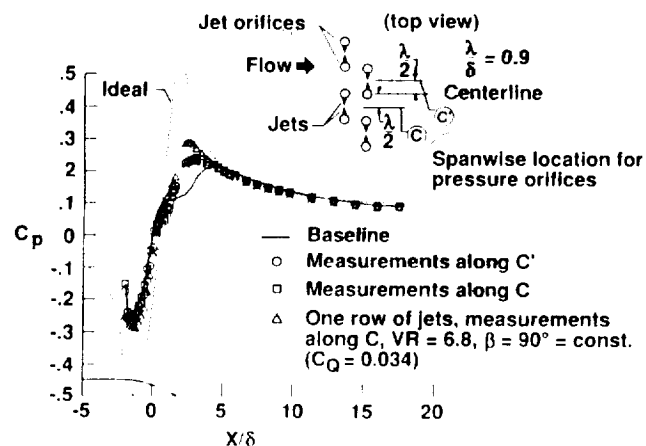Figure 17. Pressure distributions at two spanwise locations for a double row of co-rotating jet vortex generators with $\alpha = 15°$, $\beta = 90°$, $D_o/\theta = 0.24$, VR = 6.8, and $C_Q = 0.034$.

Figure 18. Oil flow visualization for a double row of co-rotating jet vortex generators with $\alpha = 15°$, $\beta = 90°$, $D_o/\theta = 0.24$, VR = 6.8, and $C_Q = 0.034$.

Figure 19. Pressure distributions at two spanwise locations for a double row of counter-rotating jet vortex generators with $\alpha = 15°$, $D_o/\theta = 0.24$, VR = 3.4, and $C_Q = 0.017$.

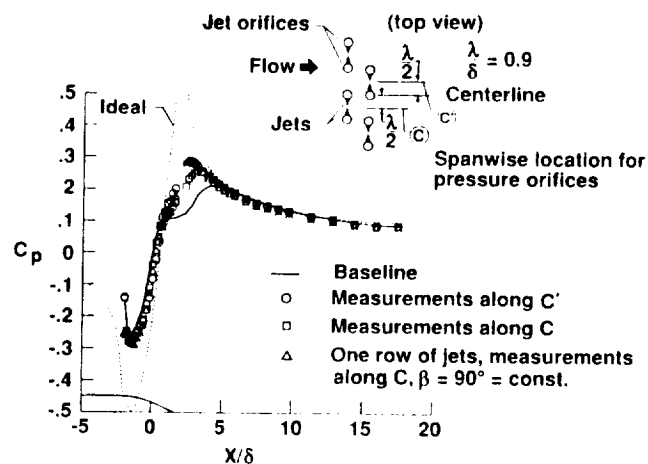Figure 20. Pressure distributions at two spanwise locations for a double row of counter-rotating jet vortex generators with $\alpha = 15°$, $D_o/\theta = 0.24$, VR = 6.8, and $C_Q = 0.034$.
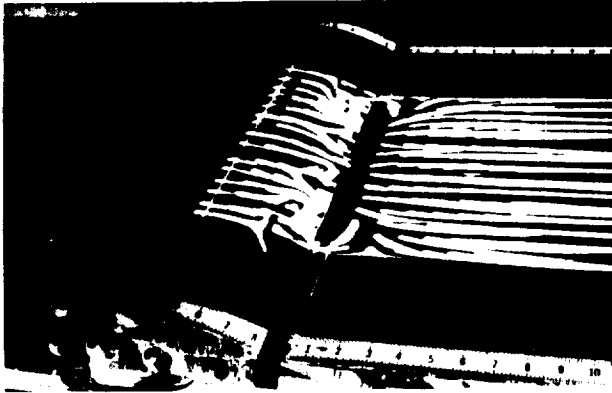
Figure 21. Oil flow visualization for a double row of counter-rotating jet vortex generators with α = 15°, D_o/θ = 0.24, VR = 6.8, and C_Q = 0.034.
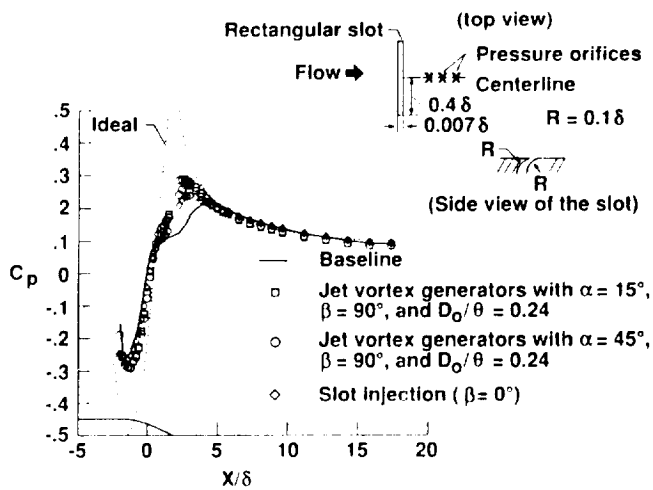

Figure 22. Pressure distributions for rectangular-slot injection (0.13x23.4 mm) and jet vortex generators with equal flow areas, VR = 6.8, and C_Q = 0.034.
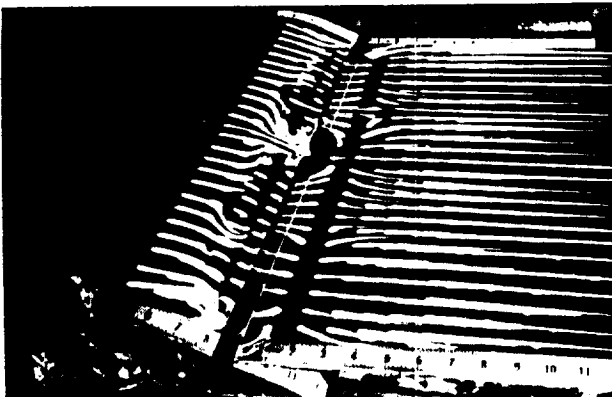

Figure 23. Oil flow visualization for rectangular-slot injection (0.13x23.4 mm) with VR = 6.8 and C_Q = 0.034.